# Virtual-Flux-Based Predictive Direct Power Control of Three-Phase PWM Rectifiers With Fast Dynamic Response

Yongsoo Cho, *Student Member, IEEE*, and Kyo-Beum Lee, *Senior Member, IEEE*

***Abstract*—This paper proposes a power predictive control (PPC) method for three-phase pulse width modulated rectifiers without a proportional-integral controller. The proposed PPC method calculates the optimized voltage vector by analyzing the relationship between the virtual flux, active power, converter voltage, and filter parameters. Thus, an overshoot does not occur and the fast and accurate power control becomes possible. The predictive algorithm computes the power error that would be produced by applying each vector and selects the one that contributes the minimum error. The simulation and experimental results prove that the proposed method provides an excellent steady-state performance and quick dynamic response.**

***Index Terms*—AC/DC power conversion, direct power control, power predictive control (PPC), pulse width modulation (PWM) rectifiers, space vector modulation (SVM), power ripple reduction, virtual flux.**

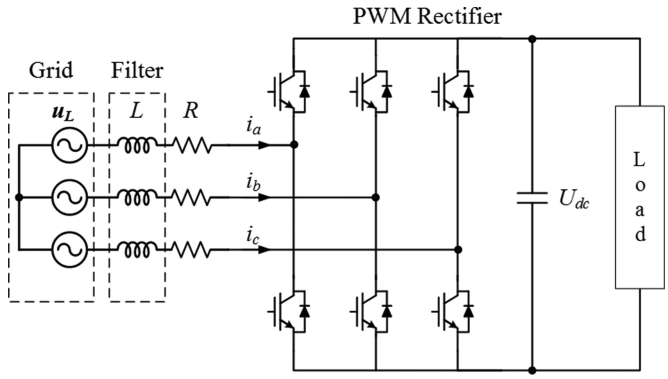


Fig. 1. Three-phase PWM rectifier system.

## I. Introduction

CONVENTIONAL AC/DC converters usually use a diode rectifier. The diode rectifier is simple, robust, and low cost. However, while containing many low-order harmonics, the diode rectifier requires a separate device to process the surplus energy on the load side. Because of this disadvantage, a pulse width modulation (PWM) converter with a switching device is used instead of a diode rectifier. Because a three-phase PWM converter (see Fig. 1) can sinusoidally control the input current, the converter can reduce the harmonic components of the input current and control the phase of the input current for the input voltage. In addition, not only can the converter maintain a stable dc-link voltage for the load change, but it can also regenerate the surplus power from the load side toward the ac source, thus achieving high efficiency and a high power factor (PF). Active research regarding the control method of the three-phase PWM rectifier is being conducted [1]–[3].

Four control methods for the three-phase PWM rectifier are available [1]: voltage-oriented control, voltage-based direct power control [4], virtual-flux-oriented control, and virtual-flux-based direct power control (VF-DPC) [1]. Among them, the VF-DPC is similar to direct torque control that is used for motor drives. Because VF-DPC does not require processes such as reference frame transformation, and phase lock loop is possible through the virtual flux, it is an algorithm that is simple for applications [5]–[8].

The VF-DPC calculates the active and reactive powers by measuring the input current and the estimated virtual flux, and instantaneously performs power control by using the hysteresis comparator and the switching table. Some of the most prominent advantages of this method are fast and excellent power dynamics during an abrupt change of the load or changes in the instantaneous reference with low sensitivity to nonideal supply voltages, and the lack of a pulse width modulator [5]. However, there are also some disadvantages: the magnitude of a power ripple is dependent on the magnitude of the dc-link voltage, a high sampling frequency is needed for digital implementation of hysteresis comparators, and the switching frequency varies according to the load condition. In addition, it is very difficult to realize because a very-high-performance processor is needed in order to have a very fast control period.

The usage of limited number of voltage vectors is insufficient in accurate power control. Then, a space vector modulation (SVM)-based DPC scheme has been proposed, which shows to be an effective method to reduce the power ripple [9], [10]. In the proposed method, an optimal reference voltage vector is calculated and applied to the machine using SVM. Not only can this method (produced by the reference voltage vector through the PI controller from the error between the active and reactive powers) effectively reduce power ripple, but it also has the

Manuscript received March 24, 2015; revised June 9, 2015; accepted July 1, 2015. Date of publication July 10, 2015; date of current version November 30, 2015. This work was supported by Basic Science Research Program through the National Research Foundation of Korea (NRF) funded by the Ministry of Education (2013R1A1A2A10006090). Recommended for publication by Associate Editor J. O. Ojo.

The authors are with the Department of Electrical and Computer Engineering, Ajou University, Suwon 443-749, Korea (e-mail: marine_blue@ajou.ac.kr; kyl@ajou.ac.kr).

Color versions of one or more of the figures in this paper are available online at http://ieeexplore.ieee.org.

Digital Object Identifier 10.1109/TPEL.2015.2453129

advantage of a fixed switching frequency. However, the dynamics that correspond to the abrupt load change need to adjust an adequate gain owing to influence from the gain of the PI controller. In addition, the dynamic response is slower than that of a conventional VF-DPC.

Recently, a model predictive direct power control (MPDPC) algorithm that incorporates the conventional VF-DPC algorithm with the model predictive control (MPC) algorithm has been proposed [11]–[16]. The MPDPC can achieve a good steady-state performance and quick dynamic response by selecting the optimal voltage vector. This minimizes the error between the reference power and the actual power. The optimal voltage vector is determined by a control scheme that minimizes the cost function. The cost function used in the MPC for power control generally consists of the sum of the square or absolute values from the error term of the active and reactive powers, and it is used to find an appropriate control input from the finite input set.

However, as with the VF-DPC, because the MPDPC applies one voltage vector for one control period, the active and reactive powers ripples increase [12]. Therefore, even though there are increasing numbers of studies on control techniques that divide voltage vectors for application in the system and which require precise control, this approach requires a large amount of calculation [17]–[19].

In this paper, a power predictive control (PPC) is proposed [20], [21] that discards the PI controller, and switching look-up table. This PPC analyzes the relationship between the grid voltage, virtual flux, power, and converter voltage, and selects the optimized voltage vector to apply the rectifier switching through SVM. The proposed method does not need the PI gain adjustment required by a conventional DPC-SVM. The proposed method can accurately perform the VF-DPC without an overshoot by applying voltage through the mathematical calculations, which results in excellent dynamics. The effectiveness of the proposed algorithm is verified by results obtained through simulations and experiments.

## II. Virtual-Flux-Based Predictive Model

### A. Virtual Flux and Power Estimation

Fig. 2 illustrates the vector diagram and coordinate axes under steady-state operating conditions. The $\alpha$-$\beta$ reference frame is a stationary reference frame, whereas the *d-q* reference frame is a rotating frame that is synchronized to the virtual-flux $\boldsymbol{\lambda_L}$. The grid voltage $\boldsymbol{u_L}$ $(=[u_{L\alpha}\ \ u_{L\beta}]^T)$ and the $\boldsymbol{\lambda_L}$ $(=[\lambda_{L\alpha}\ \ \lambda_{L\beta}]^T)$ equations in the stationary reference frame are

$$\boldsymbol{u_L} = R\boldsymbol{i_L} + L\frac{d\boldsymbol{i_L}}{dt} + \boldsymbol{u_{\mathrm{conv}}} \tag{1}$$

$$\boldsymbol{\lambda_L} = \int \boldsymbol{u_L} dt = \int \left(\boldsymbol{u_{\mathrm{conv}}} + R\boldsymbol{i_L}\right) dt + L\boldsymbol{i_L} \tag{2}$$

where $\boldsymbol{u_{\mathrm{conv}}}$ $(=[u_{\mathrm{conv}\alpha}\ \ u_{\mathrm{conv}\beta}]^T)$ is the converter ac-side voltage, $\boldsymbol{i_L}$ $(=[i_{L\alpha}\ \ i_{L\beta}]^T)$ is the line current, *R* is the line resistance, and *L* is the line inductance. The $\alpha$-$\beta$ components of

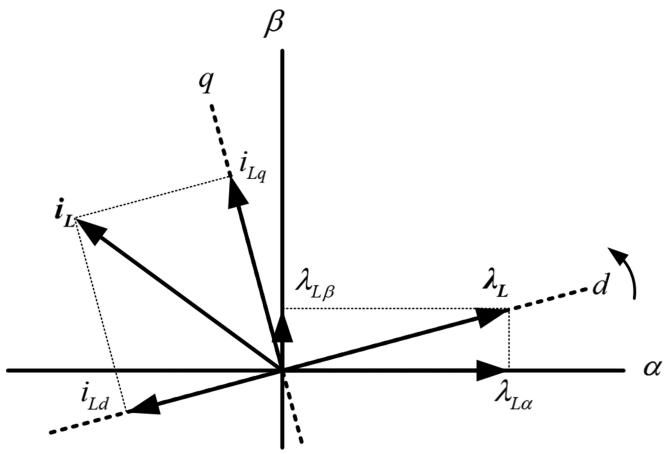


Fig. 2. Reference coordinates and vectors.

the $\boldsymbol{u_{\mathrm{conv}}}$ can be obtained from the dc-link voltage $U_{\mathrm{dc}}$ and the duty cycles of converter switching ($D_a$, $D_b$, and $D_c$) as follows [12]:

$$\begin{aligned}\boldsymbol{u}_{\mathrm{conv}} &= \begin{bmatrix} u_{\mathrm{conv}\alpha} \\ u_{\mathrm{conv}\beta} \end{bmatrix} \\ &= \begin{bmatrix} \left(\sqrt{2/3}\right) U_{\mathrm{dc}} \left(D_a - 1/2\left(D_b + D_c\right)\right) \\ \left(1/\sqrt{2}\right) U_{\mathrm{dc}} \left(D_b - D_c\right) \end{bmatrix}. \end{aligned} \tag{3}$$

For sinusoidal and balanced voltage, neglecting the $R = 0$, the instantaneous active power *P* and reactive power *Q* in a stationary frame is given by (4) and (5), respectively [6], [12]

$$P = \omega\left|\boldsymbol{\lambda_L} \times \boldsymbol{i_L}\right| = \omega\left(\lambda_{L\alpha} i_{L\beta} - \lambda_{L\beta} i_{L\alpha}\right) \tag{4}$$

$$Q = \omega\left(\boldsymbol{\lambda_L} \cdot \boldsymbol{i_L}\right) = \omega\left(\lambda_{L\alpha} i_{L\alpha} + \lambda_{L\beta} i_{L\beta}\right) \tag{5}$$

where $\omega$ is the angular frequency of $\boldsymbol{\lambda_L}$.

### B. Relationship of Voltage Vectors to the Active Power

In the analysis, the stationary reference frame is used. The PPC is based on time-varying instantaneous power. The active power differentiation is calculated from (4) as

$$\frac{dP}{dt} = \omega\left(\lambda_{L\alpha}\frac{di_{L\beta}}{dt} + \frac{d\lambda_{L\alpha}}{dt} i_{L\beta} - \lambda_{L\beta}\frac{di_{L\alpha}}{dt} - \frac{d\lambda_{L\beta}}{dt} i_{L\alpha}\right). \tag{6}$$

From (1) and (2), the changing rates of $\boldsymbol{\lambda_L}$ and $\boldsymbol{i_L}$ according to time *t*, are as follows:

$$\frac{d}{dt}\lambda_{L\alpha} = u_{\mathrm{conv}\alpha} + Ri_{L\alpha} + L\frac{di_{L\alpha}}{dt} = u_{L\alpha} \tag{7}$$

$$\frac{d}{dt}\lambda_{L\beta} = u_{\mathrm{conv}\beta} + Ri_{L\beta} + L\frac{di_{L\beta}}{dt} = u_{L\beta} \tag{8}$$

$$\frac{di_{L\alpha}}{dt} = \frac{1}{L}\left(u_{L\alpha} - u_{\mathrm{conv}\alpha} - Ri_{L\alpha}\right) \tag{9}$$

$$\frac{di_{L\beta}}{dt} = \frac{1}{L}\left(u_{L\beta} - u_{\mathrm{conv}\beta} - Ri_{L\beta}\right). \quad (10)$$

Substituting (7)–(10) into (6), the differentiated power with respect to *t* is

$$\frac{dP}{dt} = \omega\left(u_{L\alpha}i_{L\beta} - u_{L\beta}i_{L\alpha} + \lambda_{L\alpha}\frac{1}{L}\left(u_{L\beta} - u_{\mathrm{conv}\beta} - Ri_{L\beta}\right) - \lambda_{L\beta}\frac{1}{L}\left(u_{L\alpha} - u_{\mathrm{conv}\alpha} - Ri_{L\alpha}\right)\right). \quad (11)$$

By rearranging (11), the following equation is obtained:

$$\frac{dP}{dt} = \frac{\omega}{L}\left(\left(\lambda_{L\alpha} - Li_{L\alpha}\right)u_{L\beta} - \left(\lambda_{L\beta} - Li_{L\beta}\right)u_{L\alpha}\right) - \frac{R}{L}P - \frac{\omega}{L}\left(\lambda_{L\alpha}u_{\mathrm{conv}\beta} - \lambda_{L\beta}u_{\mathrm{conv}\alpha}\right). \quad (12)$$

By determining the value of $\boldsymbol{u_L}$, $\boldsymbol{\lambda_L}$, and $\boldsymbol{i_L}$, it is possible to control the active power toward a desired value by controlling voltage $\boldsymbol{u_{\mathrm{conv}}}$.

## III. Predictive Control of Power

The DPC method based on SVM calculates the reference voltage vector $\boldsymbol{u}^*$ from the errors in active and reactive powers; using these values, the converter operates using the SVM method [9]. Two main advantages of the SVM method can be realized: fixing the sampling period and realizing continuous voltage vectors. However, because the conventional DPC-SVM method uses the PI controller to calculate the control angle and the magnitude to the $\boldsymbol{u}^*$, an overshoot can occur in the power if the gain value of the PI controller is not adequately adjusted. In this paper, the proposed PPC-SVM method, which does not choose the voltage vector using the PI controller such as the conventional DPC-SVM, analyzes the relationship between *P*, $\boldsymbol{u_L}$, $\boldsymbol{\lambda_L}$, $\boldsymbol{i_L}$, and $\boldsymbol{u_{\mathrm{conv}}}$. Based on the mathematical equations, this method controls powers through the calculation of the $\boldsymbol{V}^*$; hence, the accurate active power control becomes feasible and has excellent dynamic characteristics.

### A. Proposed Power Predictive Control Strategy

Let the converter flux be $\boldsymbol{\lambda_{\mathrm{conv}}}$ ( $= [\lambda_{\mathrm{conv}\alpha}\ \lambda_{\mathrm{conv}\beta}]^T$). From (7) and (8), neglecting the voltage drop on line resistance, the increment of $\boldsymbol{\lambda_{\mathrm{conv}}}$ can be calculated as

$$\lambda_{\mathrm{conv}\alpha} = \int (u_{L\alpha} - Ri_{L\alpha})dt - Li_{L\alpha} \approx \int u_{L\alpha}dt - Li_{L\alpha} \approx (\lambda_{L\alpha} - Li_{L\alpha}) \quad (13)$$

$$\lambda_{\mathrm{conv}\beta} = \int (u_{L\beta} - Ri_{L\beta})dt - Li_{L\beta} \approx \int u_{L\beta}dt - Li_{L\beta} \approx (\lambda_{L\beta} - Li_{L\beta}). \quad (14)$$

Therefore, by substituting (13) and (14) into (12)

$$\frac{d}{dt}P = \frac{\omega}{L}\left(\lambda_{\mathrm{conv}\alpha}u_{L\beta} - \lambda_{\mathrm{conv}\beta}u_{L\alpha}\right) - \frac{R}{L}P - \frac{\omega}{L}\left(\lambda_{L\alpha}u_{\mathrm{conv}\beta} - \lambda_{L\beta}u_{\mathrm{conv}\alpha}\right). \quad (15)$$

Suppose that during one DSP the control period $T_s$. On the basis of (15), we can deduce the change rate of *P*, which are influenced by the $\boldsymbol{u_{\mathrm{conv}}}$ as follows:

$$\begin{aligned}\Delta P &= \left(\frac{\omega}{L}\left(\lambda_{\mathrm{conv}\alpha}u_{L\beta} - \lambda_{\mathrm{conv}\beta}u_{L\alpha}\right) - \frac{R}{L}P - \frac{\omega}{L}\left(\lambda_{L\alpha}u_{\mathrm{conv}\beta} - \lambda_{L\beta}u_{\mathrm{conv}\alpha}\right)\right)\cdot T_s \\ &= \left(\frac{\omega}{L}\left(\lambda_{\mathrm{conv}\alpha}u_{L\beta} - \lambda_{\mathrm{conv}\beta}u_{L\alpha}\right) - \frac{R}{L}P\right)\cdot T_s - \frac{\omega}{L}\left|\boldsymbol{\lambda_L}\times\boldsymbol{u_{\mathrm{conv}}}\right|\cdot T_s \\ &= \left(\frac{\omega}{L}\left(\lambda_{\mathrm{conv}\alpha}u_{L\beta} - \lambda_{\mathrm{conv}\beta}u_{L\alpha}\right) - \frac{R}{L}P\right)\cdot T_s - \frac{\omega}{L}\left|\boldsymbol{\lambda_L}\right|\cdot\left|\boldsymbol{u_{\mathrm{conv}}}\right|\sin\theta\cdot T_s. \end{aligned} \quad (16)$$

Let the magnitude of reference voltage vector $\boldsymbol{u}^*$ is the maximum voltage that can be generated from the converter during $T_s$. From (16), the angle of $\boldsymbol{u}^*$ can be obtained as follows:

$$\theta^* = \arcsin\left(\frac{-\Delta P + \left(\frac{\omega}{L}\lambda_{\mathrm{conv}\alpha}u_{L\beta} - \lambda_{\mathrm{conv}\beta}u_{L\alpha} - \frac{R}{L}P\right)\cdot T_s}{\frac{\omega}{L}\left|\boldsymbol{\lambda_L}\right|\cdot\left|\boldsymbol{u_{\mathrm{conv}}}\right|\cdot T_s}\right). \quad (17)$$

The purpose of the angle is to decide the proper direction of $\boldsymbol{u}^*$ for driving the power error ΔP to zero.

### B. Power Ripple Reduction Method

The $\boldsymbol{u}^*$ is obtained previously. The magnitude of $\boldsymbol{u}^*$ that can be chosen in the converter will be restricted. Its restricted use of the voltage vector is unsuitable for accurate power control. In particular, the magnitude of the power ripple is influenced by the voltage magnitude of the dc link such as VF-DPC. The proposed power ripple reduction method of the PPC-SVM is a two-step design. The first step, as shown in Fig. 3, is to determine the magnitude of the reference voltage in the *d*-axis $u_d^*$ by using converter flux error $\Delta\lambda_{\mathrm{conv}}$ to apply the nonzero voltage vector $\boldsymbol{u_k}$ as required by the converter flux control. Then, the second step is to modify the reference voltage vector $\boldsymbol{u^*_{\mathrm{mod}}}$, which was previously determined by predictive $\boldsymbol{u}^*$, by calculating the angle and the magnitude of $\boldsymbol{u}^*$ that possess $\Delta P$ of the same amount within the magnitude of $u_d^*$. The predictive algorithm computes $\Delta P$ by applying each vector and selecting the one that contributes to the minimum error. From (13) and (14), $\boldsymbol{\lambda_{\mathrm{conv}}}$ can be processed as an integration of $\boldsymbol{u_{\mathrm{conv}}}$. Neglecting the voltage drop on line resistance, the magnitude of the voltage vector required for the flux control can be obtained as

$$\boldsymbol{u^*_{\mathrm{mod}}} = \begin{bmatrix} u_d^* \\ u_q^* \end{bmatrix} \approx \begin{bmatrix} \Delta\lambda_{\mathrm{conv}}T_s^{-1} \\ |\boldsymbol{u}^*|\sin\theta^* \end{bmatrix}. \quad (18)$$

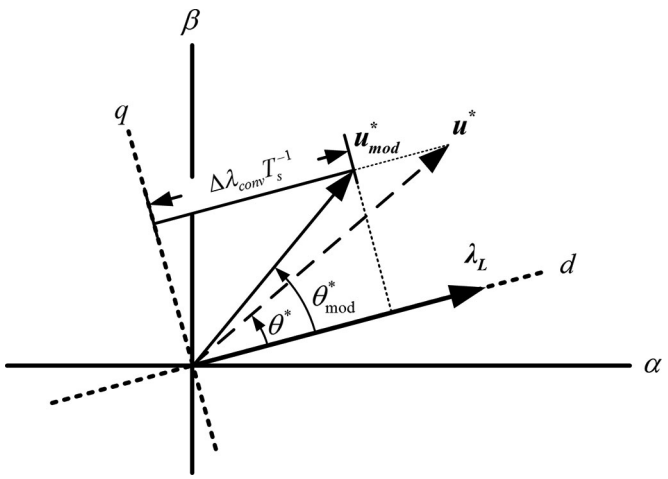


Fig. 3. Power ripple reduction strategy.

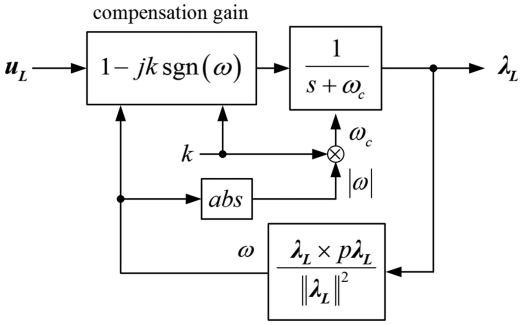


Fig. 4. LPF with compensation.

TABLE I
AREA VOLTAGE VECTOR

| Converter Flux | Active Power | Selected Areas |
|---|---|---|
| $\lambda_{conv}\uparrow$ | $P\downarrow$ | Area I |
| $\lambda_{conv}\downarrow$ | $P\downarrow$ | Area II |
| $\lambda_{conv}\downarrow$ | $P\uparrow$ | Area III |
| $\lambda_{conv}\uparrow$ | $P\uparrow$ | Area IV |

The converter flux error can be defined as

$$\Delta\lambda_{\mathrm{conv}} = \lambda^*_{\mathrm{conv}} - |\boldsymbol{\lambda_{conv}}|\,. \tag{19}$$

The acquired magnitude of $\boldsymbol{u^*_{mod}}$ is set by the magnitude of $\boldsymbol{u^*_d}$ and $\boldsymbol{u^*_q}$. By using the previously obtained $\boldsymbol{u}^*$ and $\Delta\lambda_{\mathrm{conv}}$, the magnitude and angle of $\boldsymbol{u^*_{mod}}$ that produce the same variation in active power can be obtained by using the trigonometric equation as follows:

$$\begin{aligned}|\boldsymbol{u^*_{mod}}| &= \sqrt{(u^*_d)^2 + (u^*_q)^2} \\ &= \sqrt{(\Delta\lambda_{\mathrm{conv}}T_s^{-1})^2 + (|\boldsymbol{u}^*|\sin\theta^*)^2} \end{aligned}\tag{20}$$

$$\theta^*_{\mathrm{mod}} = \arcsin\left(\frac{|\boldsymbol{u}^*|}{|\boldsymbol{u^*_{mod}}|}\sin\theta^*\right). \tag{21}$$

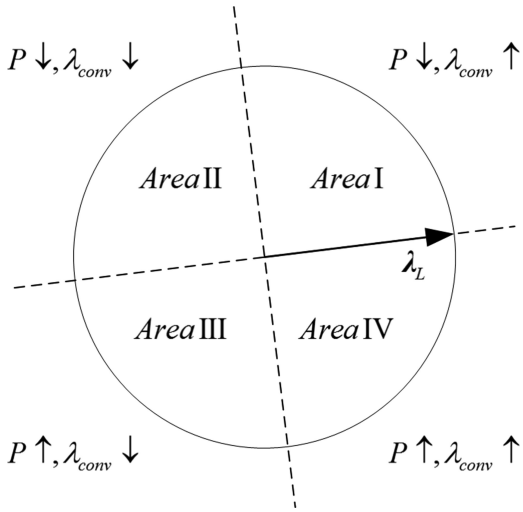


Fig. 5. Phase plane division for control of active power and converter flux.

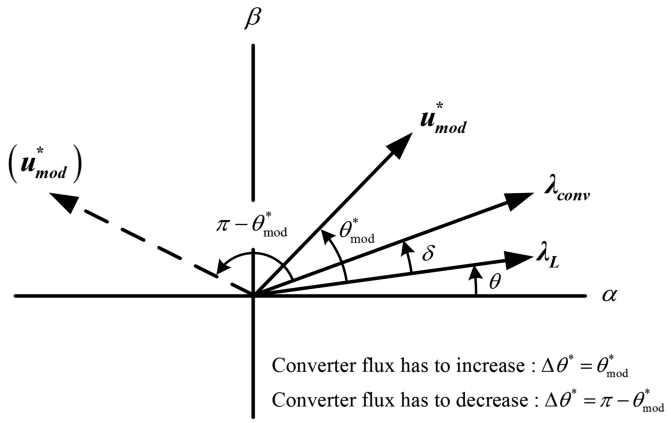


Fig. 6. Control of the converter flux.

The voltage vector that ensures minimum power ripple is selected based on the PPC-SVM algorithm.

### C. Virtual-Flux Estimation

Estimating the virtual flux has been investigated in many works [8], [22], [23]. In this paper, a simple and effective method for $\boldsymbol{\lambda_L}$ estimation is employed. This method was introduced in [22] and [23]. In practical digital implementation, the pure integration in (2) is sensitive to dc drift in the input. A natural method is to incorporate a high-pass filter (HPF) behind the pure integrator. This is equivalent to implementing a low-pass filter (LPF). Although the introduction of an HPF eliminates the dc drift, it also results in errors in both magnitude and phase. The amplitude and phase errors between the pure integrator and LPF in the steady state of a sine waveform are obtained as follows:

$$\Delta G = \frac{\sqrt{\omega^2+\omega_c^2}}{\omega} \tag{22}$$

$$\Delta\theta = \arctan\frac{\omega}{\omega_c} - \frac{\pi}{2} = -\arctan\frac{\omega_c}{\omega} \tag{23}$$

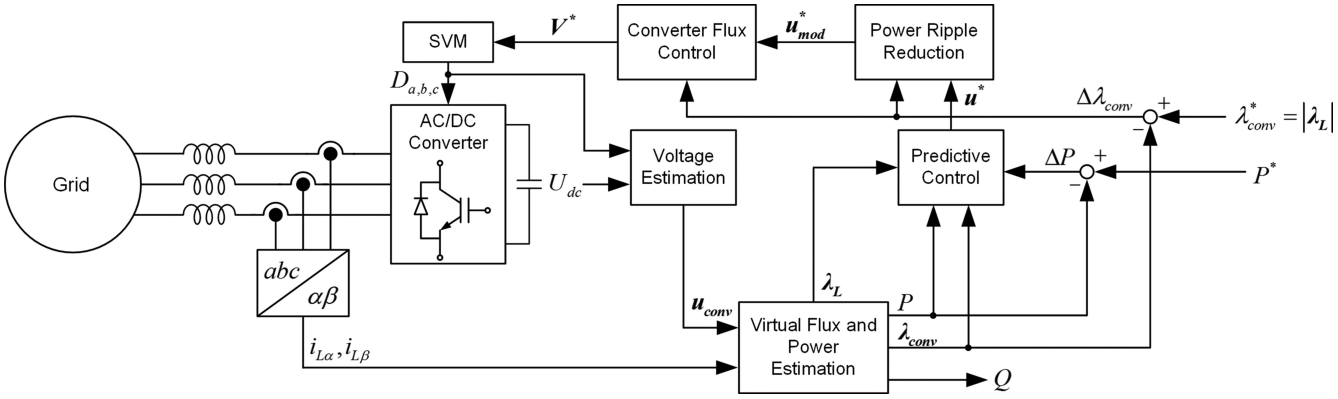


Fig. 7. Block diagram of the PPC-SVM.

where $\omega$ is the synchronous frequency of $\boldsymbol{\lambda_L}$ and $\omega_c$ is the cutoff frequency of the LPF. To eliminate the steady-state errors caused by the LPF, a compensation term is needed, i.e.

$$G = \Delta G e^{\Delta\theta} = \frac{\sqrt{\omega^2 + \omega_c^2}}{\omega} e^{-\arctan\frac{\omega_c}{\omega}} = 1 + \frac{\omega_c}{j\omega}. \quad (24)$$

To improve the performance, the cutoff frequency should vary with the grid frequency $\omega$, i.e., $\omega_c = k\omega$, where $k$ is typically chosen as $k = 0.1 \ldots 0.5$. The transient behavior is good if $k$ is small, but a higher value of $k$ allows more dc offset in the measurements. Pure integration is achieved by choosing $k = 0$. The synchronous frequency $\omega$ can be calculated from $\boldsymbol{\lambda_L}$ as

$$\omega = \frac{\boldsymbol{\lambda_L} \times p\boldsymbol{\lambda_L}}{\|\boldsymbol{\lambda_L}\|^2} = \frac{\lambda_{L\alpha} u_{L\beta} - \lambda_{L\beta} u_{L\alpha}}{\lambda_{L\alpha}^2 + \lambda_{L\beta}^2} \quad (25)$$

where $p$ is the differential operator. The structure of the $\boldsymbol{\lambda_L}$ estimator is shown in Fig. 4. The compensation is carried out before the LPF component to improve the dynamic performance. The simple complex-valued compensation gain is used instead of calculating the phase error and the gain error as in [23].

### D. Control of the Converter Flux

The $\boldsymbol{\lambda_L}$ synchronized to the *d-q* reference frame is shown in Fig. 2. The *d*-axis represents the $\boldsymbol{\lambda_L}$, and the *q*-axis represents the *P*. These two dotted lines split the *d-q* reference frame into four quadrants, as shown in Fig. 5. Each zone is characterized by the sign of the *P* and $\boldsymbol{\lambda_{conv}}$ as shown in Table I. When the $\boldsymbol{u}_{\rm conv}$ is located inside one of them, the *P* and $\boldsymbol{\lambda_{conv}}$ can be increase or decrease depending on selected areas. For example, when both of the *P* and $\boldsymbol{\lambda_{conv}}$ need to be increased, the selected voltage vector is located in the area IV.

Angle $\theta^*_{\rm mod}$ of $\boldsymbol{u^*_{mod}}$ in (21) ensures an accurate control of the *P*. Fig. 6 shows the relationship between $\boldsymbol{u^*_{mod}}$, $\boldsymbol{\lambda_L}$, and $\boldsymbol{\lambda_{conv}}$. When *P* decreases, $\boldsymbol{\lambda_{conv}}$ leads $\boldsymbol{\lambda_L}$ by angle $\delta$. By contrast, when *P* increases, $\boldsymbol{\lambda_{conv}}$ lags $\boldsymbol{\lambda_L}$ by angle $\delta$. Additionally, if the phase difference between $\boldsymbol{u^*_{mod}}$ and $\boldsymbol{\lambda_{conv}}$ is within $\pm 90°$, the magnitude of $\boldsymbol{\lambda_{conv}}$ increases; otherwise, it decreases. Hence, the angle of $\boldsymbol{u^*_{mod}}$ to control $\boldsymbol{\lambda_{conv}}$ can be determined in the following manner:

1) the magnitude of $\boldsymbol{\lambda_{conv}}$ must increase, $\Delta\theta^* = \theta^*_{\rm mod}$ ;
2) the magnitude of $\boldsymbol{\lambda_{conv}}$ must decrease, $\Delta\theta^* = \pi - \theta^*_{\rm mod}$ .

TABLE II
SIMULATION PARAMETERS

| Parameter | Value |
|---|---|
| Line–line voltage [$U_{L-L}$] | $380 V_{\rm rms}$ |
| Grid frequency [*f*] | 60 Hz |
| Line resistance [*R*] | 50 mΩ |
| Line inductance [*L*] | 10 mH |
| DC-link voltage [$U_{\rm dc}$] | 600 V |
| DC-link capacitor [*C*] | 1700 $\mu$F |

The $\boldsymbol{u^*_{mod}}$ angle of the proposed PPC becomes $\Delta\theta^*$. Therefore, after obtaining the angle increment, the output reference voltage vector $\boldsymbol{V}^*$ can be expressed in the following equation in polar coordinates as

$$\boldsymbol{V}^* = |\boldsymbol{u^*_{mod}}| \cdot e^{j(\theta + \Delta\theta^*)}. \quad (26)$$

The final selected reference voltage vector can be synthesized by using two adjacent voltage vectors and zero voltage vector.

### E. Block Scheme of Predictive Power Control

The block scheme of the virtual-flux-based PPC-SVM system is shown in Fig. 7. First, the output current is detected to calculate $\boldsymbol{i_L}$ in the stationary reference frame. In addition, $\boldsymbol{u_L}$ can be obtained from (1) and (3). Then, in the virtual flux and power estimation block, *P*, *Q*, and $\boldsymbol{\lambda_L}$ are estimated using (4), (5), and (25). The process of calculating the $\boldsymbol{\lambda_L}$ is clearly presented in Fig. 4. In the predictive control block, the angle of $\boldsymbol{u}^*$ that sets $\Delta P$ to zero is calculated, where the maximum duty of obtained from $P^*$, *P*, $\boldsymbol{\lambda_{conv}}$, and $\Delta P$ by calculating (17). This angle is the phase difference between $\boldsymbol{u}^*$ and $\boldsymbol{\lambda_L}$. From the ripple minimization controller, the magnitude of modify reference voltage vector is determined by $\Delta\lambda_{\rm conv}$ and $\boldsymbol{u}^*$ using (18), and $\boldsymbol{u}^*$ is corrected by recalculating the magnitude and angle of $\boldsymbol{u^*_{mod}}$ using (20) and (21). The converter flux controller create the final $\boldsymbol{V}^*$ using the hysteresis control technique with calculated $\boldsymbol{u^*_{mod}}$, $\theta^*$, and $\Delta\lambda_{\rm conv}$. Finally, the recreated $\boldsymbol{V}^*$ is used to control the converter switching using the SVM method.

Using such a method, power control for reducing power ripple can be performed. In the case of the control for the reactive power *Q*, if the reference value of $\boldsymbol{\lambda_{conv}}$ and the value of $\boldsymbol{\lambda_L}$

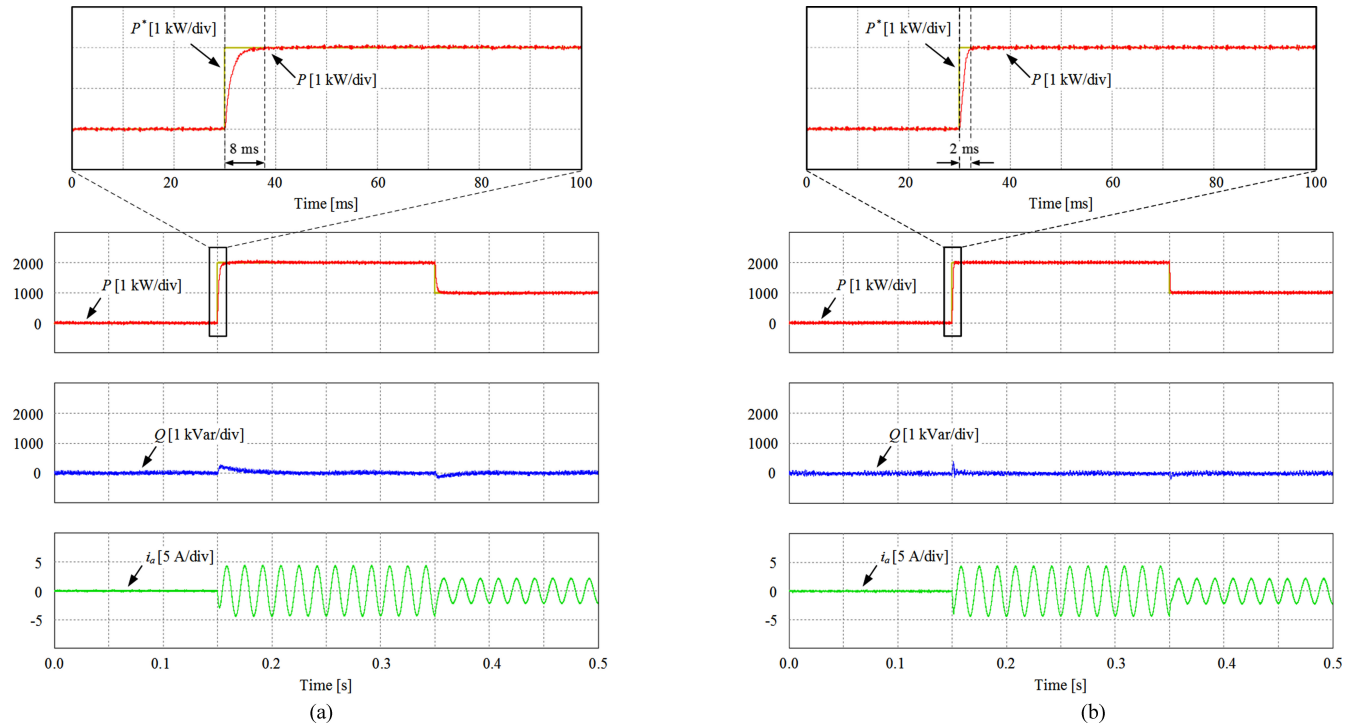


Fig. 8. Simulation result under step change of the reference power: (a) conventional DPC-SVM and (b) proposed PPC-SVM.

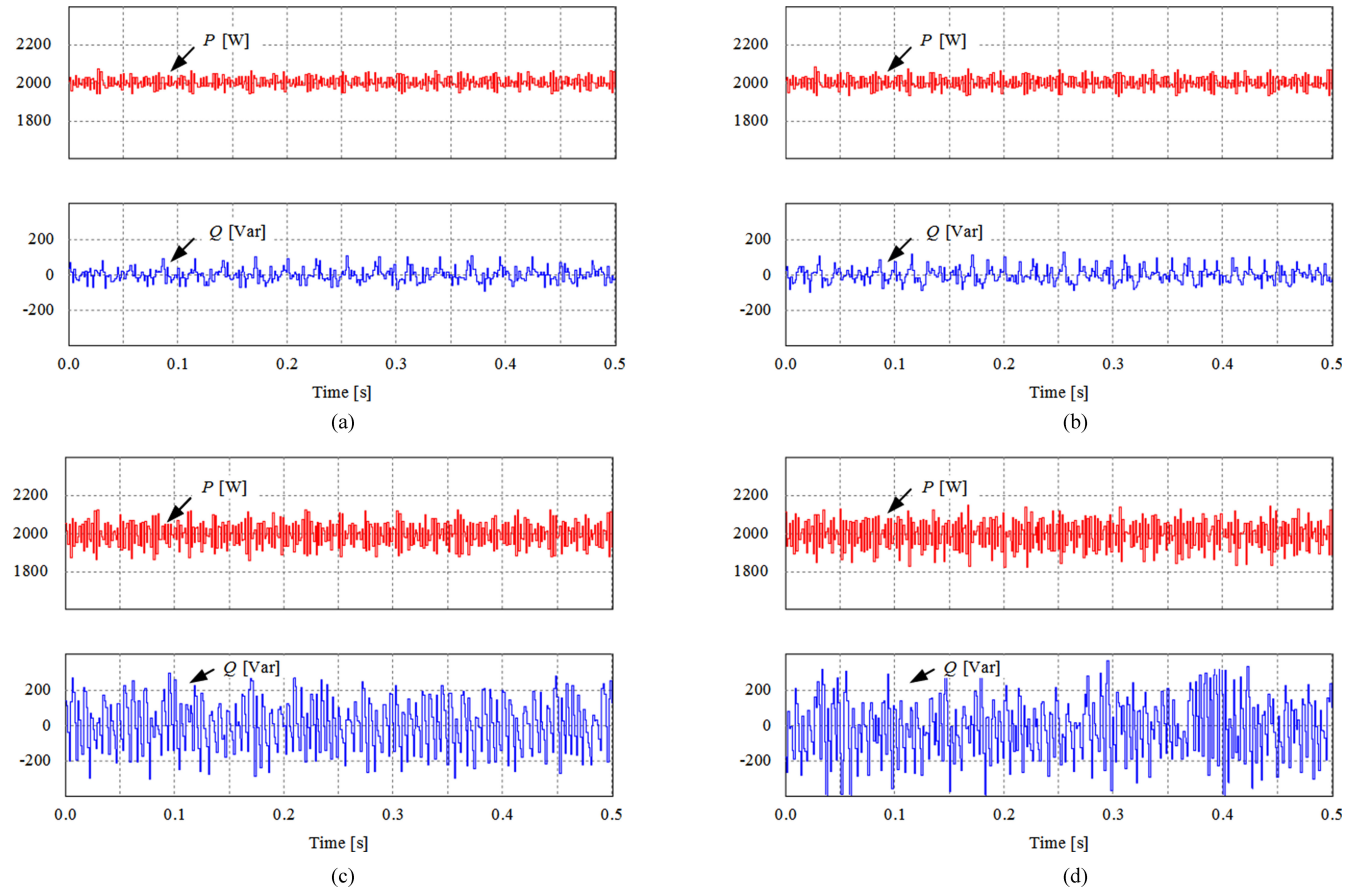


Fig. 9. Simulation results of active power and reactive power for the proposed PPC-SVM: (a) $L = 5$ mH, (b) $L = 10$ mH (real value), (c) $L = 15$ mH, and (d) $L = 20$ mH.

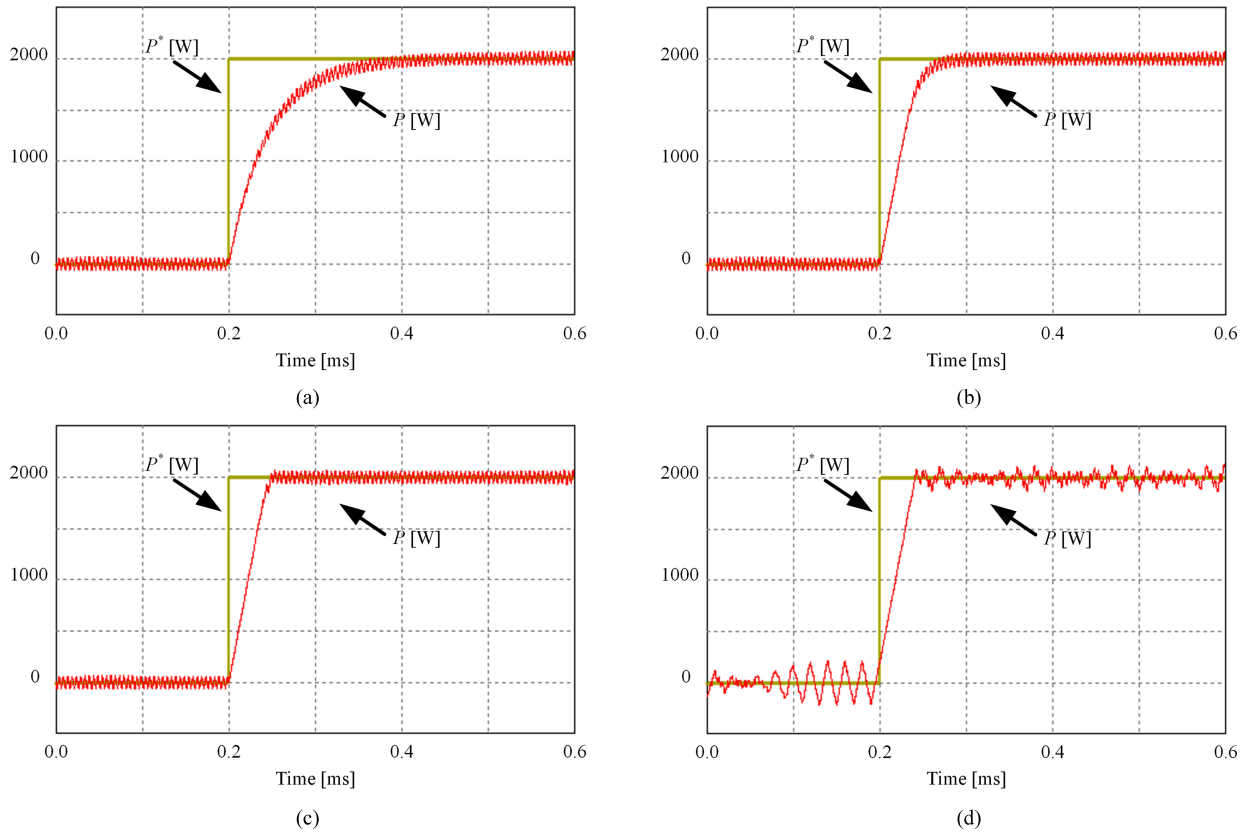


Fig. 10. Simulation result of the active power step response for the proposed PPC-SVM: (a) L = 2 mH, (b) L = 5 mH, (c) $L$ = 10 mH (real value), and (d) $L$ = 20 mH.

are the same, $Q$ is controlled to become 0. On the other hand, it is possible to perform the reactive power control by varying the reference value of $\boldsymbol{\lambda}_{\mathbf{conv}}$ in order to increase or decrease $Q$.

## IV. Simulation Results

The system was simulated using the PSIM software tool to prove the effectiveness of the proposed control method. The simulation was carried out under the conditions listed in Table II.

The sampling time for the PPC-SVM control scheme is 128 $\mu$s, and the switching frequency of the converter is set to 7.8 kHz in accordance with the experimental setting. In order to perform the control with $Q$ as 0, the simulation was carried out by setting the reference value of $\lambda_{\mathbf{conv}}$ and the value of $\boldsymbol{\lambda}_{\boldsymbol{L}}$ to be the same.

Fig. 8 shows the simulation results of the power dynamic control performances of the conventional DPC-SVM and the proposed PPC-SVM with a power step that changes from 0 to 2 kW at 0.15 s and from 2 to 1 kW at 0.35 s. As shown in Fig. 8 (both power control strategies), because the proposed method's dynamic performance takes 2 ms, it is 8 ms faster (approximately four times) than the conventional DPC-SVM without the overshoot.

To examine the robustness of the proposed PPC-SVM, a series of simulations are completed where the line inductance is different from the real value. These results are shown in Fig. 9. It is seen that if the inductance value used in the control is 50% of the real value [see Fig. 9(a)], the ripple in the active and reactive powers will be almost the same. On the other hand, if the inductance value used in the control is increased to 100% [see Fig. 9(d)], the active power ripple increases from 100 to 300 W (a threefold increase). For the reactive power, the ripple increases significantly from 100 to 600 Var (a sixfold increase).

Fig. 10 shows the response of the active power for the proposed PPC-SVM when the actual inductance in control differs from the real value. Fig. 10(a) and (b) shows the value of the control parameter is smaller than the actual inductance. In that case, the magnitude of power ripple is almost same as Fig. 10(c), but the power dynamics decrease in the transient-state interval. On the other hand, Fig. 10(d) shows the value of the control parameter is larger than the actual inductance. In that case, the power dynamic response is similar to Fig. 10(c), but the magnitude of power ripple is increase. Therefore, it is possible to adjust the control response though the changing the $L$ value. Through the simulation results although the difference in the inductance value affects the system performance of the proposed PPC-SVM it is verified that the difference of the inductance, from $-20\%$ to 200%, does not affect the stability of the system.

Fig. 11 shows the dc-link voltage transient value when an external load (2 kW) is applied to the dc link at 0.15 s. The dc-link voltage only decreases by 5 V after the load is connected, and its reference is achieved again in only 0.1 s after the load

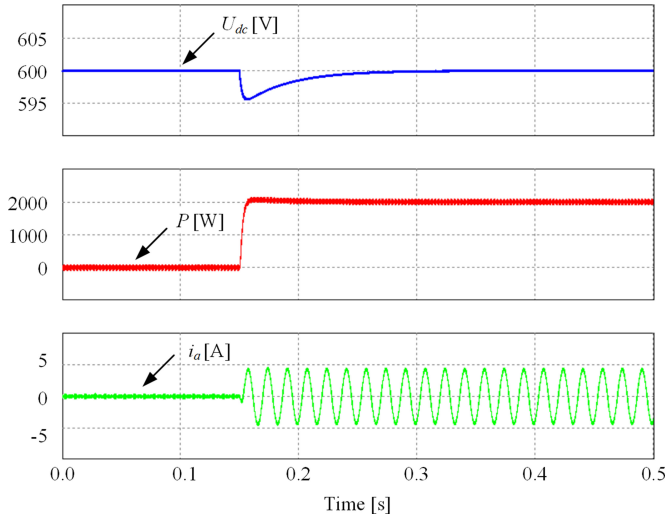


Fig. 11. Simulation result of the step change of the load in the proposed PPC-SVM.

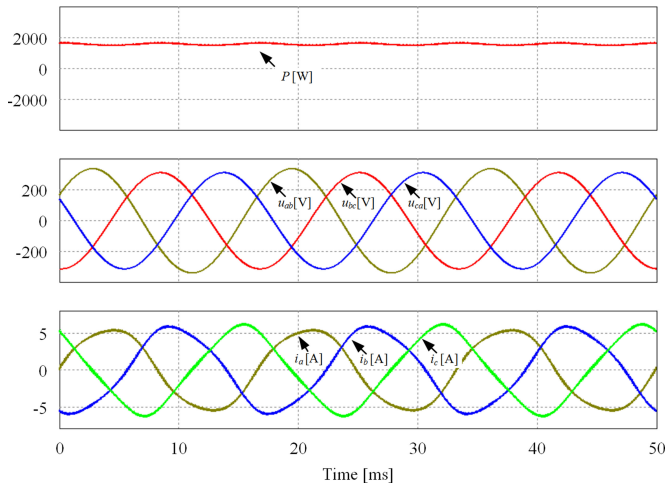


Fig. 12. Simulation result of the proposed PPC-SVM under unbalanced grid voltage.

change, thus a good voltage regulation is ensured. It is seen that during this dynamic process showing strong robustness against external load disturbance.

Fig. 12 shows the simulation results for the proposed PPC-SVM when the unbalanced grid voltages. From top to bottom, the curves shown in Fig. 11 are active power, three-phase grid voltages, and three-phase grid currents. The amplitude of the three-phase line to line voltage is $240\,V_{ab(\mathrm{rms})}$, $220\,V_{bc(\mathrm{rms})}$, and $220\,V_{ca(\mathrm{rms})}$, respectively. When the grid voltages unbalanced, although the grid currents are distorted, active power still tracks reference well. The result proves that the proposed PPC-SVM can work well under both balanced and unbalanced grid condition.

## V. Experimental Results

The proposed control strategy was further validated by an experiment that used a laboratory setup, as shown in Fig. 13. The setup consists of the following devices: a three-phase intelligent

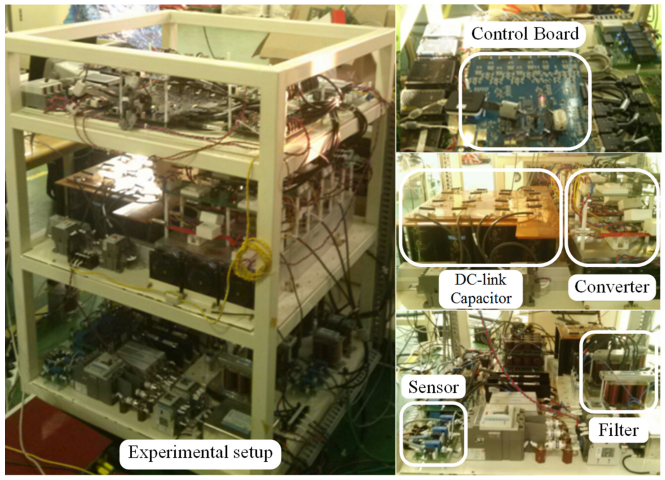


Fig. 13. Experimental setup of ac/dc PWM converter.

insulated-gate bipolar transistor power module as the inverter, a dc power source, and a three-phase $L$ filter. A DSP 28346 control board was employed to implement a real-time algorithm coding using the C language for the control. The parameters of the experiment were the same as those presented in Table II.

It is a comparison of the number of clock that is consumed at the time control of the proposed method and the conventional method. According to the comparison, the number of clocks of the conventional algorithm is 5175, and the number of clocks of the proposed algorithm is 4758. Because the clock speed of TMS320C28346 is 300 MHz, the calculation time decreases from 17.25 to 15.86 $\mu$s, which is by about 9.2%. Thus, the complexity in terms of the calculation of proposed PPC-SVM is smaller than of the conventional DPC-SVM.

Fig. 14(a) and (b) shows the dynamic responses of the conventional DPC-SVM and proposed PPC-SVM, respectively, when the reactive power is controlled at 0 Var and the active power is varied from 0 to 2 kW at 0.15 s and from 2 to 1 kW at 0.35 s. The figures show the active power $P$, reactive power $Q$, and a-phase line current $\boldsymbol{i_a}$. As shown in Fig. 14(a), it takes 11 ms for the dynamic performance to reach the reference value without the existence of an overshoot. It is possible to adjust the response by the gain tuning the PI controller. However, if the response becomes faster, the overshoot increases; if the overshoot decreases, the response becomes slower. Therefore, some type of tradeoff must take place. However, in Fig. 14(b), because the proposed method's dynamic performance takes 4 ms, it is 7 ms faster than the conventional DPC-SVM without the existence of an overshoot. As a result, when the reference power shifts, the arrival time changes from 11 to 4 ms, indicating that the response time of the proposed PPC-SVM is reduced by 36% compared with the conventional DPC-SVM.

Fig. 15 shows the experimental waveform for the case where the inductance value in control is different from the actual inductance value (10 mH). This is carried out in order to verify the robustness of the proposed PPC-SVM. The figure shows the experimental waveforms when the inductance values in control are $-50\%$ and 200%. As shown in Fig. 15(a) and (b), both active and reactive powers will be almost the same. If the inductance value

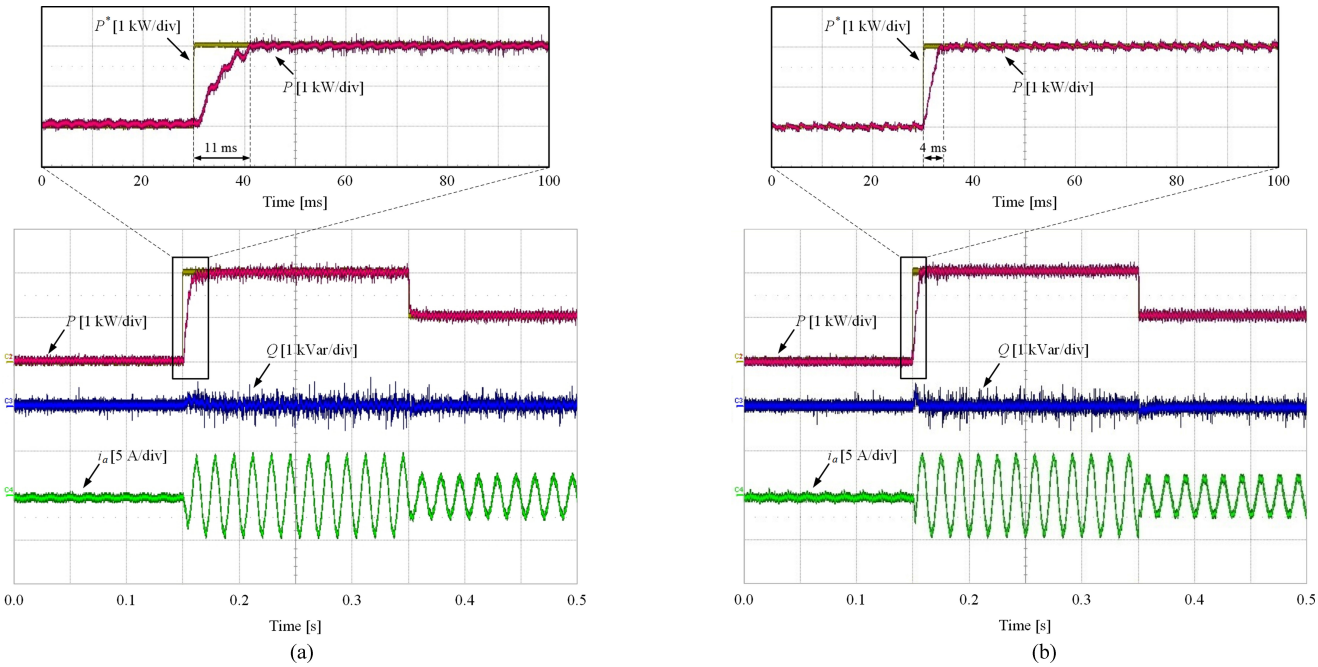


Fig. 14. Experimental result under step change of the reference power: (a) conventional DPC-SVM and (b) proposed PPC-SVM.

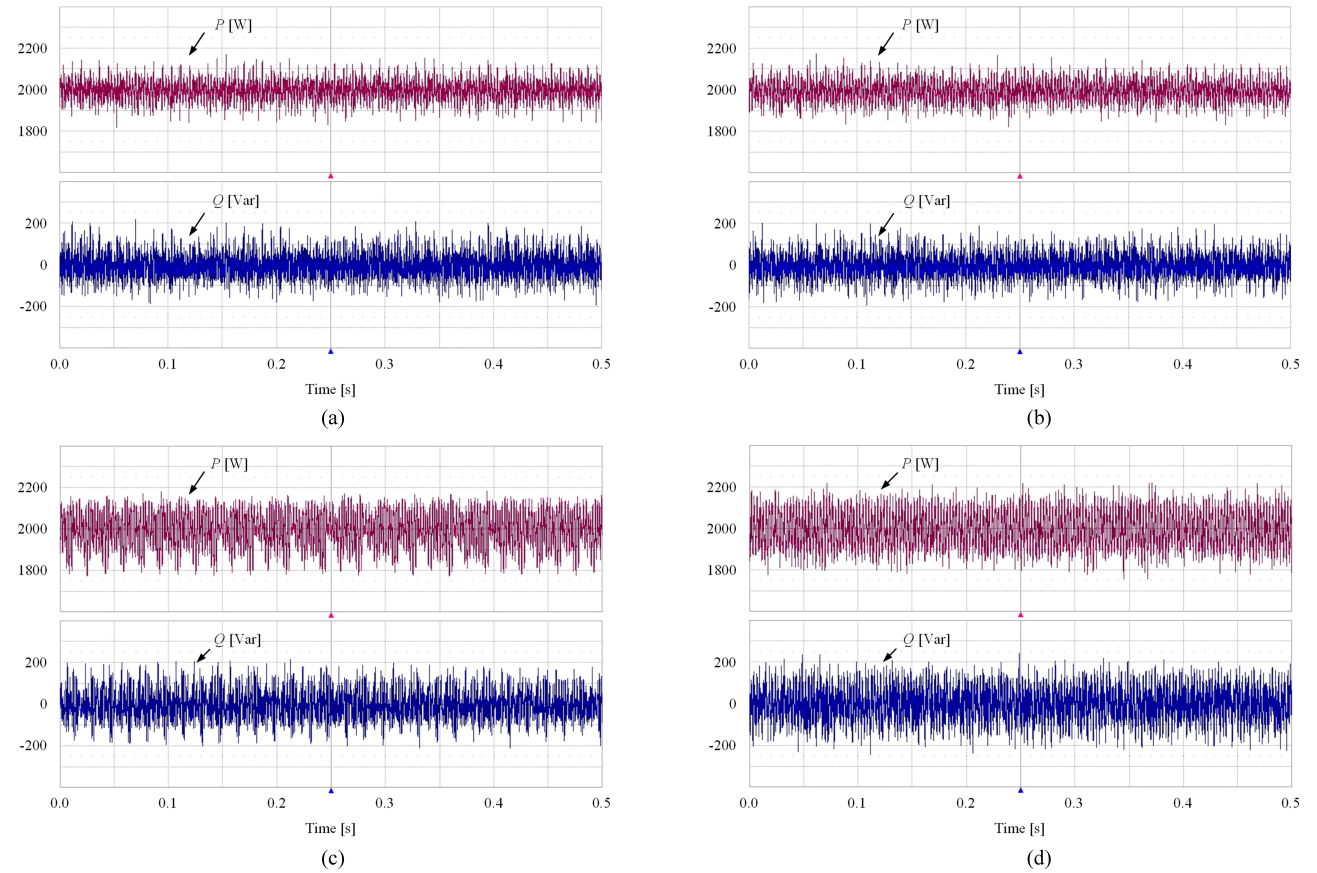


Fig. 15. Experimental results of active power and reactive power for the proposed PPC-SVM: (a) $L = 5$ mH, (b) $L = 10$ mH (real value), (c) $L = 15$ mH, and (d) $L = 20$ mH.

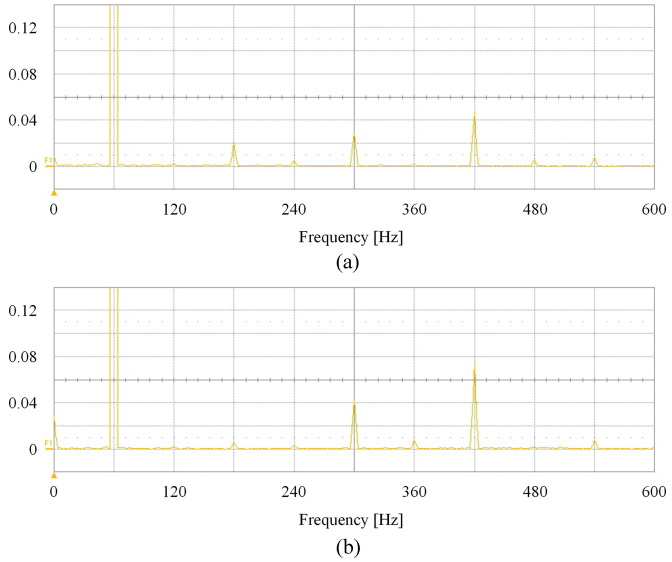


Fig. 16. Frequency spectrum of the line current: (a) conventional DPC-SVM and (b) proposed PPC-SVM.

used in the control are 150% and 200%, the ripples of active and reactive power increase significantly, as shown in Fig. 15(c) and (d), respectively. However, the unit power factor operation is maintained. From Fig. 15, it can be said that although the steady-state performance deteriorates when the inductance varies, the proposed algorithm is still stable and controllable at least in the range from $-50\%$ to 100% of inductance variations. To maintain the control performance, it is better to use an online inductance identification technique, as shown in [12] and [24].

The frequency spectra for line current using different control strategies are shown in Fig. 16. It can be seen that the magnitude of third harmonic of the proposed method is smaller than that of the conventional method, but the magnitude of fifth and seventh harmonics of the proposed method slightly increase.

The proposed PPC-SVM is compared with the conventional DPC-SVM in terms of efficiency, PF, and total harmonic distortion (THD) of $\boldsymbol{i_L}$, as shown in Fig. 17. Fig. 17(a) and (b) shows that the proposed method exhibits a slightly higher efficiency and PF than the conventional method. However, the THD of the proposed method is higher than that of the conventional method in the low power region, as shown in Fig. 17(c).

Fig. 18 shows the experimental waveform for the responses to external load disturbance under the condition of the closed dc-link voltage control. An external load of 2 kW is suddenly applied to the PWM rectifier. From top to bottom, the curves shown in Fig. 18 are dc-link voltage, active power, and line current. There is only small drop in the dc-link voltage and it returns to its reference value quickly without any undesirable overshoot and oscillation, exhibiting strong robustness against external load disturbance.

Fig. 19 shows the performance of the proposed PPC-SVM under unbalanced and distorted voltage supply. Unbalanced three-phase voltage supply is very common in a weak ac system. The unbalanced phenomenon can be arising from single-phase loads

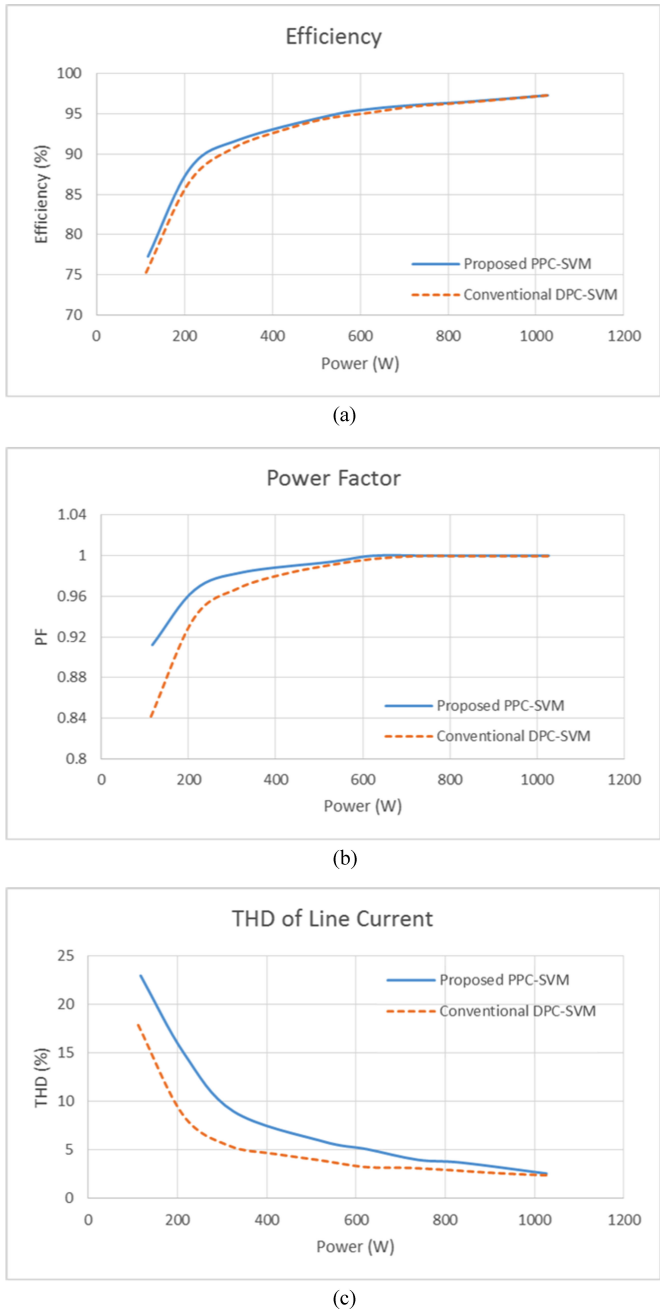


Fig. 17. Comparison results of conventional DPC-SVM and proposed PPC-SVM: (a) efficiency, (b) PF, and (c) THD of $\boldsymbol{i_L}$.

that are unevenly distributed in the grid system. Actual grid voltages during phase unbalance can be seen in the second waveform of Fig. 19 and those voltages are the actual grid measurements that the control system uses. As a result, it was confirmed that the proposed algorithm can be controlled without problems even under unbalanced ac mains voltages as seen in first and third waveform of Fig. 19. The current has low-order harmonics like fifth and seventh due to the grid voltage harmonics. Thus, the three-phase grid currents are distorted and unbalanced. In order to control the three-phase current to a sinusoidal wave, it is better to use an unbalanced grid voltage compensation technique, as shown in [25].

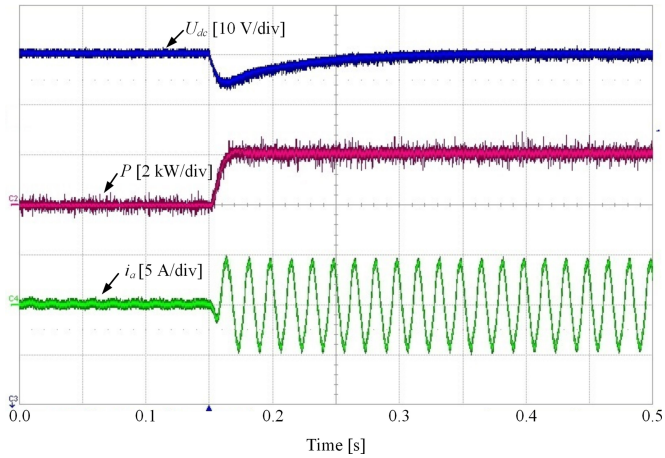


Fig. 18. Experimental result of the step change of the load in the proposed PPC-SVM.

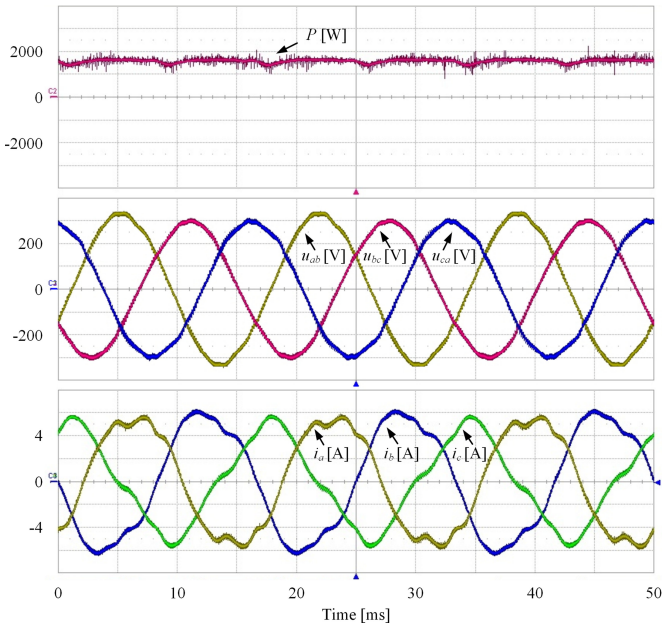


Fig. 19. Performance of the proposed PPC-SVM under unbalanced and distorted voltage supply.

## VI. Conclusion

This paper proposed a PPC-SVM method with excellent transient performance. The PPC-SVM strategy has been discussed based on the discrete-time state-space model. A power dynamic equation is developed for the analysis of real-time power behavior. The prediction scheme uses the changing rates, according to time $t$, in the virtual flux and the line current, together with voltage vectors to achieve accurate power control. Unlike the conventional DPC-SVM method, the proposed method without the PI controller has an advantage in that the dynamics are improved. The simulation and experimental results demonstrated that the proposed method effectively improves the dynamics compared to the conventional DPC-SVM.

## Reference

[1] M. Malinowski, M. Kazmierkowski, and A. Trzynadlowski, "A comparative study of control techniques for PWM rectifiers in ac adjustable speed drives," *IEEE Trans. Power Electron.*, vol. 18, no. 6, pp. 1390–1396, Nov. 2003.

[2] J. Hu, L. Shang, Y. He, and Z. Z. Zhu, "Direct active and reactive power regulation of grid-connected DC/AC converters using sliding mode control approach," *IEEE Trans. Power Electron.*, vol. 26, no. 1, pp. 210–222, Jan. 2011.

[3] J.-S. Lee and K.-B. Lee, "Carrier-based discontinuous PWM method for VIENNA rectifiers," *IEEE Trans. Power Electron*, vol. 30, no. 6, pp. 2896–2900, Jun. 2015.

[4] S. Vazquez, J. A. Sanchez, J. M. Carrasco, J. I. Leon, and E. Galvan, "A model-based direct power control for three-phase power converters," *IEEE Trans. Ind. Electron.*, vol. 55, no. 4, pp. 1647–1657, Apr. 2008.

[5] M. Malinowski, M. P. Kazmierkowski, S. Hansen, F Blaabjerg, and G. D Marques, "Virtual flux based direct power control of three-phase PWM rectifiers," *IEEE Trans. Ind. Appl.*, vol. 37, no. 4, pp. 1019–1027, Jul./Aug. 2001.

[6] D. Zhi, L. Xu, and B. W. Williams, "Improved direct power control of grid-connected DC/AC converters," *IEEE Trans. Power Electron.*, vol. 24, no. 5, pp. 1280–1292, May 2009.

[7] J. H. Kim, S. T. Jou, D. K. Choi, and K. B. Lee, "Direct power control of three-phase boost rectifiers by using a sliding-mode scheme," *J. Power Electron.*, vol. 13, no. 6, pp. 1000–1007, Nov. 2013.

[8] J. Norniella, J. M. Cano, G. A. Orcajo, C. H. Rojas, J. F. Pedrayes, M. F. Cabanas, and M. G. Melero, "Improving the dynamics of virtual-flux-based control of three-phase active rectifiers," *IEEE Trans. Ind. Electron.*, vol. 61, no. 1, pp. 177–187, Jan. 2014.

[9] M. Malinowski, M. Jasinski, and M. P. Kazmierkowski, "Simple direct power control of three-phase PWM rectifier using space-vector modulation (DPC-SVM)," *IEEE Trans. Ind. Electron.*, vol. 51, no. 2, pp. 447–454, Apr. 2004.

[10] A. Bouafia, J.-P. Gaubert, and F. Krim, "Predictive direct power control of three-phase pulse width modulation (PWM) rectifier using space-vector modulation (SVM)," *IEEE Trans. Power Electron.*, vol. 25, no. 1, pp. 228–236, Jan. 2010.

[11] S. A. Larrinaga, M. A. R. Vidal, E. Oyarbide, and J. R. T. Apraiz, "Predictive control strategy of DC/AC converters based on direct power control," *IEEE Trans. Ind. Electron.*, vol. 54, no. 3, pp. 1261–1271, Jun. 2007.

[12] P. Antoniewicz and M. Kazmierkowski, "Virtual-flux-based predictive direct power control of ac/dc converters with online inductance estimation," *IEEE Trans. Ind. Electron.*, vol. 55, no. 12, pp. 4381–4390, Dec. 2008.

[13] D. E. Quevedo, R. P. Aguilera, M. A. Perez, P. Cortes, and R. Lizana, "Model predictive control of an AFE rectifier with dynamic references," *IEEE Trans. Power Electron.*, vol. 27, no. 7, pp. 3128–3136, Jul. 2012.

[14] Y. Zhang, W. Xie, Z. Li, and Y. Zhang, "Model predictive direct power control of a PWM rectifier with duty cycle optimization," *IEEE Trans. Power Electron.*, vol. 28, no. 11, pp. 5343–5351, Nov. 2013.

[15] Z. Song, W. Chen, and C. Xia, "Predictive direct power control for three-phase grid-connected converters without sector information and voltage vector selection," *IEEE Trans. Power Electron.*, vol. 29, no. 10, pp. 5518–5531, Oct. 2014.

[16] D.-K. Choi and K.-B. Lee, "Dynamic performance improvement of AC/DC converter using model predictive direct power control with finite control set," *IEEE Trans. Ind. Electron.*, vol. 62, no. 2, pp. 757–767, Feb. 2015.

[17] M. E. Romero, M. M. Seron, and G. C. Goodwin, "A combined model predictive control/space vector modulation (MPC-SVM) strategy for direct torque and flux control of induction motors," in *Proc. Ind. Electron. Soc. Conf.*, Nov. 2011, pp. 1674–1679.

[18] W. J. Choi, E. Lee, and K.-B. Lee, "A novel MPC-SVM strategy for direct torque flux control of an induction motor drive system using a matrix converter," in *Proc. IEEE Int. Conf. Ind. Technol.*, Feb/Mar. 2014, pp. 181–186.

[19] Y. Cho, W. J. Choi, and K.-B. Lee, "Model predictive control using a three-level inverter for induction motors with torque ripple reduction," in *Proc. IEEE Int. Conf. Ind. Technol.*, Feb/Mar. 2014, pp. 181–192.

[20] Y. Cho, K.-B. Lee, J.-H. Song, and Y. I. Lee, "Torque-ripple minimization and fast dynamic scheme for torque predictive control of permanent-magnet synchronous motors," *IEEE Trans. Power Electron.*, vol. 30, no. 4, pp. 2182–2190, Apr. 2015.

[21] Y. Cho and K.-B. Lee, "Virtual-flux-based power predictive control of three-phase PWM rectifiers using space-vector modulation," in *Proc. Energy Convers. Congr. Expo.*, Sep. 2014, pp. 993–998.
[22] M.-H. Shin, D.-S. Hyun, S.-B. Cho, and S.-Y. Choe, "An improved stator flux estimation for speed sensorless stator flux orientation control of induction motors," *IEEE Trans. Power Electron.*, vol. 15, no. 2, pp. 312–318, Mar. 2000.
[23] M. Hinkkanen and J. Luomi, "Modified integrator for voltage model flux estimation of induction motors," *IEEE Trans. Ind. Electron.* vol. 50, no. 4, pp. 818–820, Aug. 2003.
[24] S. Kwak, U.-C. Moon, and J.-C. Park, "Predictive-control-based direct power control with an adaptive parameter identification technique for improved AFE performance," *IEEE Trans. Power Electron*, vol. 29, no. 11, pp. 6178–6187, Nov. 2014.
[25] Y. Zhang and C. Qu, "Direct power control of a pulse width modulation rectifier using space vector modulation under unbalanced grid voltages," *IEEE Trans. Power Electron.*, vol. 30, no. 10, pp. 5892–5901, Oct. 2015.

**Yongsoo Cho** (S'12) received the B.S. degree in electrical and computer engineering from Ajou University, Suwon, Korea, in 2012, where he is currently working toward the Ph.D. degree.

His research interests include electric machine drives, grid-connected systems, and power conversion.

**Kyo-Beum Lee** (S'02–M'04–SM'10) received the B.S. and M.S. degrees in electrical and electronic engineering from the Ajou University, Suwon, Korea, in 1997 and 1999, respectively, and the Ph.D. degree in electrical engineering from the Korea University, Seoul, Korea, in 2003.

From 2003 to 2006, he was with the Institute of Energy Technology, Aalborg University, Aalborg, Denmark. From 2006 to 2007, he was with the Division of Electronics and Information Engineering, Chonbuk National University, Jeonju, Korea. In 2007, he joined the School of Electrical and Computer Engineering, Ajou University. His research interests include electric machine drives, renewable power generations, and electric vehicle applications.

Dr. Lee is an Associate Editor of the IEEE TRANSACTIONS ON POWER ELECTRONICS, the *Journal of Power Electronics*, and *the Journal of Electrical Engineering and Technology*.